Pergamon

Chaos, Solitons & Fractals, Vol. 10, No. 4–5, pp. 693–700, 1999

0960-0779/99/$ - see front matter

PII: S0960-0779(98)00017-4

Pattern Formation in a Nonlinear Optical System: the Effects of Nonlocality

P. L. RAMAZZA, S. BOCCALETTI*, A. GIAQUINTA, E. PAMPALONI, S. SORIA[1] and F. T. ARECCHI[2]

Istituto Nazionale di Ottica, I50125 Florence, Italy

Abstract—We discuss the role of nonlocal interactions in determining the mechanisms of pattern formation and selection in a nonlinear system formed by a Liquid Crystal Light Valve inserted in an optical feedback loop. We present experimental results, and compare them with the predictions of a linear stability analysis of the equations governing the system.
Nonlocality is introduced in the system via a lateral transport of a length Δx of the feedback signal. The value of the transport length plays a key role in determining the symmetry of the selected pattern in systems with both focusing and defocusing nonlinearity. In the defocusing case, the spatial wavelength of the pattern is also affected by the value of the transport length. © 1999 Elsevier Science Ltd. All rights reserved

1. INTRODUCTION

Pattern formation in nonlinear optical systems driven out of thermodynamical equilibrium has been widely discussed and demonstrated both in active and in passive optical devices [1]. The mechanism leading to pattern forming instabilities in optics is not unique. Therefore different physical agents, e.g. diffraction, diffusion, material nonlinearities, boundary conditions, determine the scale and the symmetry of the pattern occurring in different systems.

Here we report experimental and theoretical results about the role played by some nonlocal interactions [2,3], in affecting the pattern formation in a system formed by a Liquid Crystal Light Valve (LCLV) inserted in an optical feedback loop [4]. In the absence of nonlocality this system is equivalent to a Kerr slice with optical feedback [5]. The pattern forming instability arises in this case from the interplay of diffraction, diffusion and material nonlinearity.

In the case of a system with large Fresnel number, the symmetry of the selected pattern depends on the nonlinearity [6], while its typical scale is determined by diffraction and diffusion. If the diffractive scale $\sqrt{\lambda L}$, where λ is the optical wavelength and L is the free propagation distance, is much larger than the diffusive scale l_d, then the role of diffusion in determining the selected scale is negligible, and the pattern wavenumber is of the order of the diffractive scale. The most typical result for such a system is the formation of hexagons [6–8], due to the presence of quadratic nonlinearities, at a wavelength $\Lambda = \sqrt{2\lambda l}$ or $\Lambda = \sqrt{2\lambda l/3}$, for a Kerr medium with focusing or defocusing nonlinearity respectively.

Nonlocal interactions can be introduced in systems of the kind considered here e.g. via a rotation [9–11] or a translation [12–15] of the feedback signal. In all the cases, the presence of nonlocalities strongly affect the scenario of pattern formation. In the following we report some

*Also at Institut Non Lineaire de Nice-Sophia Antipolis, France.
[1]Permanent address: Dept. E.C.M., Universitat de Barcelona, Spain.
[2]Also at Department of Physics, University of Florence, I-50125 Florence, Italy.

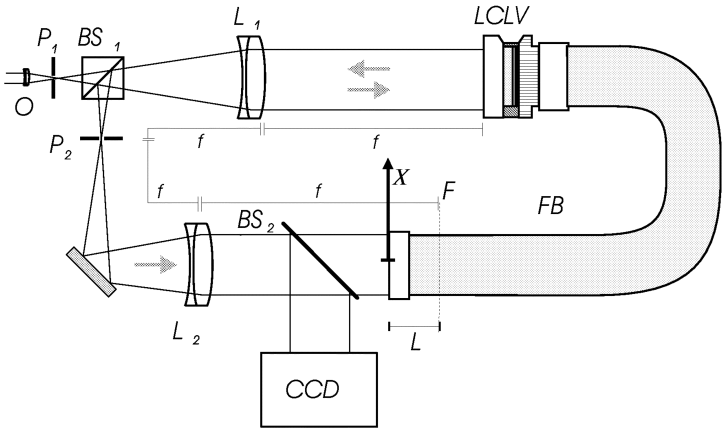

Fig. 1. Experimental setup. O=microscope objective; P_1, P_2=pinholes; BS_1, BS_2=beam splitters; $LCLV$=liquid crystal light valve; L_1, L_2=lenses of $f = 25$ *cm* focal length; FB=fiber bundle; CCD=videocamera; L=free propagation length; X=direction of transport. The $4f$ configuration of the feedback loop provides a 1 to 1 imaging of the front plane of the LCLV on the F plane.

of the most significant results obtained in the case in which the nonlocality is introduced via a lateral displacement Δx of the feedback signal.

2. EXPERIMENTAL RESULTS

The experimental setup shown in Fig. 1 consists of a liquid crystal light valve (LCLV) with diffractive feedback. The LCLV is a Kerr device operating in reflection. It induces on the wave reflected by its front face a phase distribution proportional to the intensity distribution of the light impinging on its rear face. The nonlinearity of the LCLV is of defocusing type.

In the present problem, however, a sign change of the propagation distance L is fully equivalent to a sign change of the nonlinearity [14]. The sign change of L is easily implemented via a proper choice of lenses inserted in the feedback loop. In these conditions, the nonlinearity of the overall system (LCLV+propagation) can be easily switched from defocusing to focusing.

In a first set of measurements [3], we keep fixed the amplitude and frequency of the voltage applied to the LCLV at $V_0 = 10$ V r.m.s. and $\nu = 1.5$ KHz respectively, and the propagation distance $L = -38$ cm (in the following we will indicate by L the modulus of the propagation length, which is actually negative). The overall nonlinearity of the system is therefore of focusing type. The input intensity is provided by an Ar^+ laser operating at $\lambda = 514$ nm.

We set the input intensity at $I_0 = 23\ \mu W/\text{cm}^2$, and gradually increase the value of Δx. The intensity patterns observed in these conditions are reported in Fig. 2 together with the far field patterns corresponding to the Fourier spectra.

For Δx close to 0, an hexagonal pattern is observed. The hexagons here are not oriented along some privileged direction, across the whole wavefront. Rather, domains with hexagons oriented along all the possible directions fill the plane, as evidenced by the fact that the Fourier spectrum (Fig. 2a′) is not made by a single hexagonal set of spots, but by many hexagonal sets angularly separated and filling almost uniformely a ring of constant radius.

In the range 70 μm$< \Delta x <$ 510 μm, a horizontal roll pattern is dominating. This structure is replaced by a square pattern for a range of Δx between 520 μm and 560 μm. A further increase of Δx results in the appearence of a very regular tiling of the plane with hexagons (600 μm$<$ $\Delta x <$ 770 μm). At variance with the hexagons observed for $\Delta x = 0$, these ones are oriented

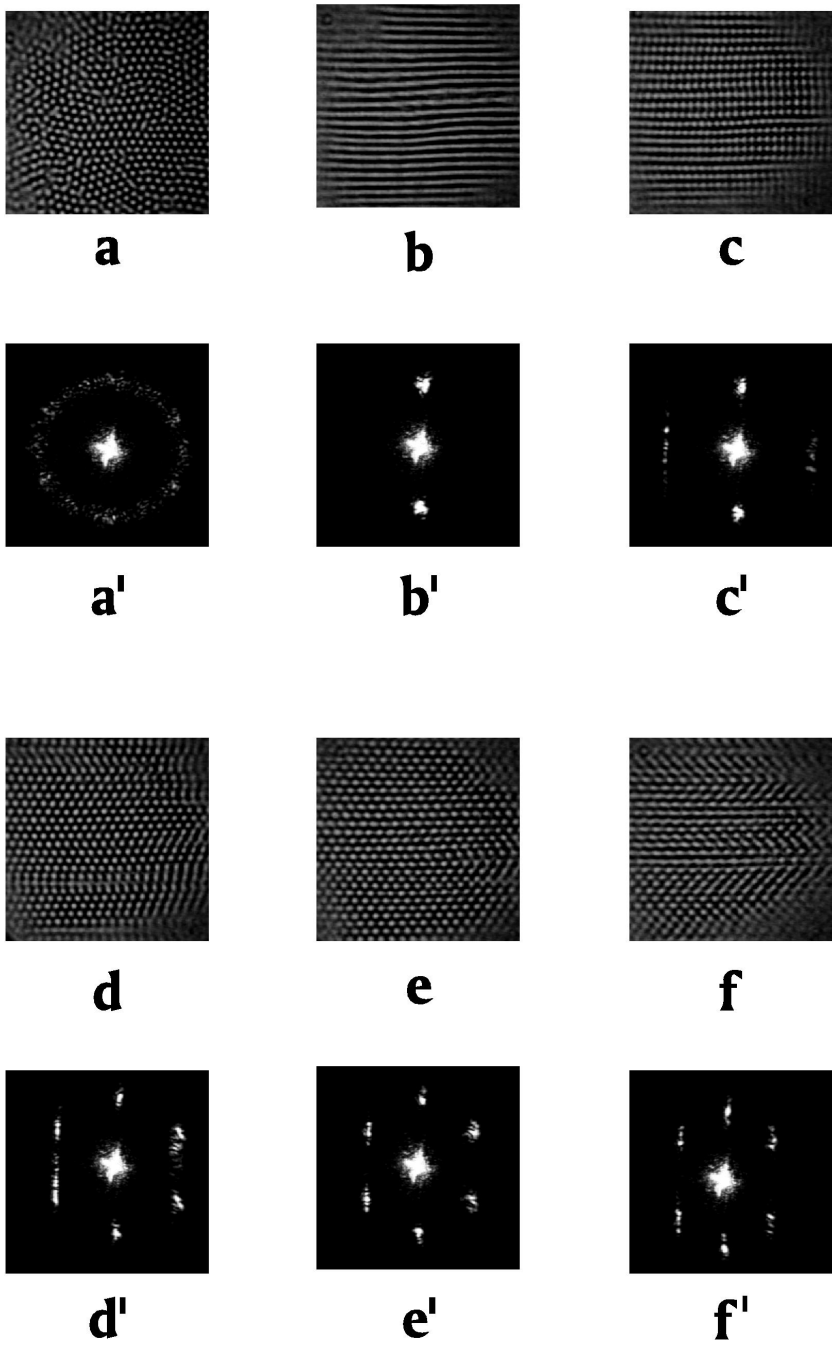

Fig. 2. Experimental near field (a–f) and far field (a′–f′) patterns in the focusing case observed at $I_0 = 23\ \mu W/cm^2$ for different Δx. (a,a′) $\Delta x = 0\ \mu$m, hexagons; (b,b′) $\Delta x = 290\ \mu$m, horizontal rolls; (c,c′) $\Delta x = 520\ \mu$m, cross rolls; (d,d′) $\Delta x = 640\ \mu$m, hexagons; (e,e′) $\Delta x = 740\ \mu$m, hexagons; (f,f′) $\Delta x = 840\ \mu$m, domain pattern. The free propagation length is $L = -38$ cm (from Ref. [3] with permission).

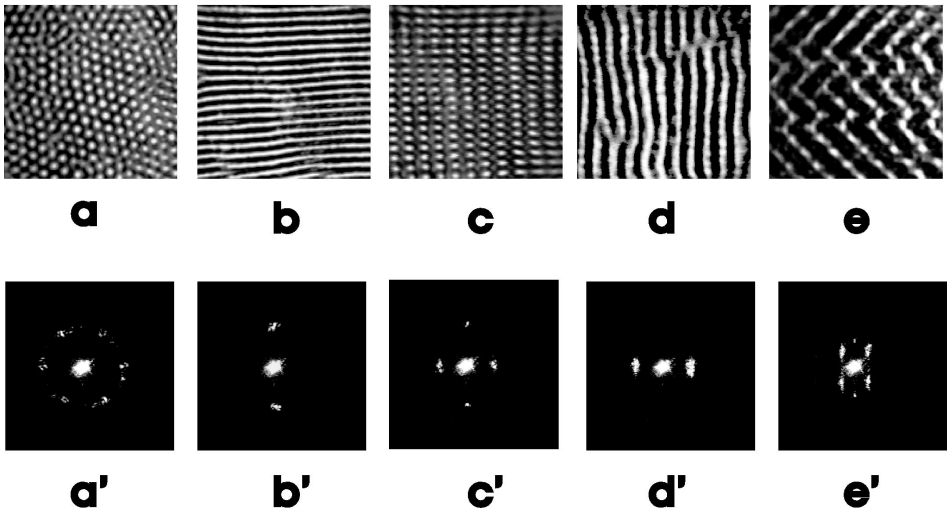

Fig. 3. Near field (above) and far field (below) patterns in the defocusing case observed for fixed input intensity ($I_0 = 72\ \mu W/cm^2$). *a,a′*: $\Delta x = 0$; *b,b′*: $\Delta x = 50\ \mu m$; *c,c′*: $\Delta x = 180\ \mu m$; *d,d′*: $\Delta x = 220\ \mu m$; *e,e′*: $\Delta x = 400\ \mu m$ (from Ref. 2 [2] with permission.

along a preferred direction, as shown by the defined spots in the Fourier space. The absence of defects in the texture is nearly total.

n general, these hexagons are nonequilateral, the ratio between their sides depending on the values of Δx. For very large values of Δx ($\Delta x > 780\ \mu$m), the hexagonal pattern breaks into domains (Fig. 2f,f′) each one filled by a different combination of the excited modes.

In a second set of measurements [2], we fixed the amplitude and frequency of the voltage applied to the LCLV to $V_0 = 12.5\ V$ r.m.s., $\nu = 4$ kHz, and the free propagation length to $L = 26$ cm. Since the propagation length is positive, the nonlinearity of the overall system is of defocusing type.

Figure 3 shows the sequence of patterns in the near field (above) and in the far field (spatial Fourier transform of the near field) (below) observed at a fixed value of input intensity $I_0 = 72\ \mu W/cm^2$ for increasing Δx .

At $\Delta x = 0$ (Fig. 3a) stationary hexagons are observed. For $20\ \mu m < \Delta x < 170\ \mu m$ (Fig. 3b), hexagons loose stability and are substituted by stationary rolls with length scale independent of Δx and oriented along Δx. At $\Delta x = 180\ \mu m$ (Fig. 3c) a cross-roll pattern formed by the coexistence of horizontal and vertical rolls emerges. Notice that horizontal and vertical rolls have different wavelengths. Vertical rolls prevail over horizontal ones for $200\ \mu m < \Delta x < 260\ \mu m$ (Fig. 3d), and display a pitch that increases for increasing Δx. These rolls drift in time in the Δx direction with a velocity which is a decreasing function of Δx. For $\Delta x \simeq 270\ \mu m$ transverse distorsions of vertical rolls begin to form, ending up with zig-zag generation (Fig. 3e).

There are appearent differences between the focusing and defocusing case with respect both to the selected pattern scale (only one scale in the focusing case, two scales in the defocusing case) and symmetry (vertical rolls exist only in the the defocusing case; hexagons for $\Delta x \neq 0$ are observed only in the focusing case). We discuss the origin of these features in the next sections.

3. COMPARISON BETWEEN EXPERIMENTS AND THEORY

The equation governing the evolution of the optical phase $\varphi(\mathbf{r}, t)$ is [3,5]:

$$\tau\frac{\partial\varphi(\mathbf{r},t)}{\partial t} = -\varphi(\mathbf{r},t) + l_d^2\nabla_\perp{}^2\varphi(\mathbf{r},t) + \alpha T_x[I_0 \mid e^{iL\nabla_\perp{}^2/2k_0}e^{i\varphi(\mathbf{r},t)}\mid^2] \tag{1}$$

Where I_0 is the input intensity, l_d and τ are respectively the diffusion length and the local relaxation time of the phase, L is the free propagation length, k_0 is the optical wavenumber, α is the Kerr coefficient ($\alpha > 0$ for focusing nonlinearity; $\alpha < 0$ for defocusing nonlinearity) and T_x is a translation operator along the x direction defined by:

$$T_x[f(x,y)] \equiv f(x+\Delta x, y) \tag{2}$$

Information on the observed scenario can be gained by linear stability analysis of (1), describing the spatiotemporal evolution of $\varphi(\mathbf{r},t)$. Temporal and spatial Fourier transformation of Eq. (1) provides relations for the real and imaginary part of the eigenvalue $\sigma_\mathbf{q} + i\omega_\mathbf{q}$ associated with the perturbations at wavevector $\mathbf{q}$:

$$\tau\sigma_\mathbf{q} = -1 - l_d^2q^2 + 2\alpha I_0\sin(\frac{q^2L}{2k_0})\cos(q\Delta x\cos\phi) \tag{3}$$

$$\tau\omega_\mathbf{q} = 2\alpha I_0\sin(\frac{q^2L}{2k_0})\sin(q\Delta x\cos\phi) \tag{4}$$

where $k_0 \equiv 2\pi/\lambda$ is the optical wavenumber, q is the modulus of $\mathbf{q}$, and ϕ is the angle between $\mathbf{q}$ and $\Delta\mathbf{x}$. The diffractive term $\sin(q^2L/2k_0)$ accounts for the free propagation within the optical feedback loop.

Let us consider first the case of $L > 0$, in which the overall nonlinearity of the system is focusing. The fundamental set of modes that maximizes the real part of the eigenvalue are expected to first destabilize at threshold. They are:

$$\phi = \pm\frac{\pi}{2}, \quad q \simeq \sqrt{\frac{\pi k_0}{L}}, \qquad \text{(horizontal rolls)} \tag{5}$$

$$\phi = 0, \pi, \quad q = q(\Delta x), \qquad \text{(vertical rolls)} \tag{6}$$

$$\phi = \pm\arccos\frac{2\pi}{q\Delta x}, \quad q \simeq \sqrt{\frac{\pi k_0}{L}}. \qquad \text{(oblique rolls)} \tag{7}$$

In writing the expressions for the unstable wavenumbers in the cases of horizontal and oblique rolls we have assumed that diffraction is dominating over diffusion in determining the length scale of the patterns [6]. This is justified by the fact that the diffusion length of the LCLV is $l_d \simeq 40\ \mu m$, so that $l_d{}^2k_0/L \simeq 0.1$.

Notice that in this case both the horizontal and the oblique roll modes lie on the band $q \simeq \sqrt{\pi k_0/L}$. As a consequence, both modes have the same threshold intensity I_{th}, hence they can coexist close to threshold, giving rise to the hexagonal pattern observed for $\Delta x \neq 0$. The threshold of the vertical roll mode is larger than I_{th} except for a single value of Δx ($\Delta x \simeq 520\ \mu$m); this explains why vertical rolls are not observed in the focusing case.

Since the eigenvalue associated with the vertical roll mode has a nonzero imaginary part, the square pattern observed around $\Delta x = 520\ \mu$m is drifting with a velocity of the order of 100 μm/sec. All the other patterns observed are stationary in time, since they arise from bifurcations of modes having zero imaginary part. This is at variance with the situation occurring in one-dimensional systems [12,15], in which drifting patterns are generic.

Figure 4 presents the theoretical threshold curves for the solutions (5)–(7), together with the experimentally measured values of the threshold intensities. The LCLV parameters are l_d =

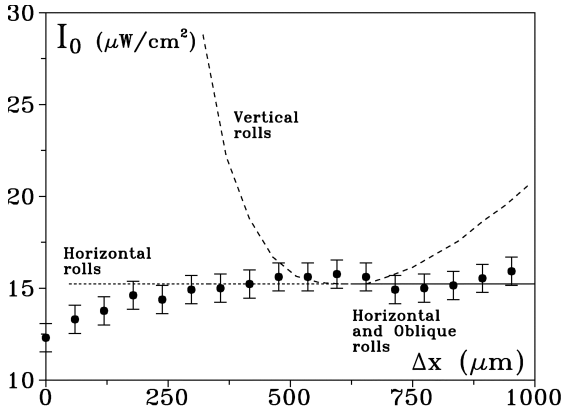

Fig. 4. Experimental and theoretical thresholds for pattern formation in the focusing case (from Ref. [3] with permission). The long (short) dashed line is the threshold calculated for vertical (horizontal) rolls, the solid line is the theoretical threshold for both horizontal and oblique rolls. The full circles represent the experimental measurements with the corresponding error bars. The Kerr coefficient used in the calculation is $\alpha = 0.072$ cm$^2/\mu W$.

40 μm, $\alpha = 0.072\ cm^2/\mu W$. The bifurcation of the hexagons at $\Delta x = 0$ is subcritical, and it requires to consider nonlinear cooperative terms between modes [6].

If we repeat the linear stability analysis for the case of defocusing nonlinearity, we obtain as the most unstable modes:

$$\phi = \pm\frac{\pi}{2}, \quad q \simeq \sqrt{\frac{3\pi k_0}{L}}, \qquad \text{(horizontal rolls)} \tag{8}$$

$$\phi = 0, \pi, \quad q = q(\Delta x), \qquad \text{(vertical rolls)} \tag{9}$$

$$\phi = \pm\arccos\frac{\pi}{q\Delta x}, \quad q \simeq \sqrt{\frac{\pi k_0}{L}}. \qquad \text{(oblique rolls)} \tag{10}$$

With respect to the analogous expression for the focusing case [16], we notice two main differences. First, the oblique roll solution exists now for $|\ \frac{q\Delta x}{\pi}\ | < 1$, instead of $|\ \frac{q\Delta x}{2\pi}\ | < 1$. Second, the horizontal and the oblique roll modes lie on different bands.

In Fig. 5 we report the marginal stability curves ($\lambda_{\mathbf{q}} = 0$) in the (Δx, I_0) plane for the solutions (8)–(10), together with the experimental instability thresholds. The theoretical curves are in fair agreement with the experimental values for a choice of the LCLV parameters $l_d = 40\ \mu m$, $\alpha = -0.0134\ cm^2/\mu W$. As in the focusing case, the only quantitative discrepancy between theory and experiments is observed for $\Delta x \simeq 0$, since for $\Delta x = 0$ the solution at threshold is the hexagonal pattern that cannot be accounted for by the linear stability analysis.

This explains the discrepancy between the measured hexagon thresholds and the ones predicted by LSA. For all the other observed patterns, the agreement between theory and experiment is good.

4. CONCLUSIONS

We have presented an experimental and theoretical investigation on the role of transport in determining the pattern formation and selection mechanisms in a nonlinear optical system. The basic mechanism whereby transport comes into play is a variation of the spatial phase relation between the phase field $\varphi(\mathbf{r})$ and the intensity field $I_{fb}(\mathbf{r})$ fed back to $\varphi(\mathbf{r})$.

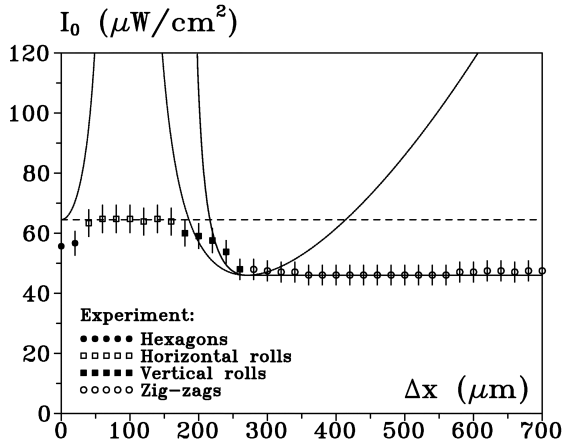

Fig. 5. Marginal stability curves $\sigma_q = 0$ in the defocusing case for horizontal rolls (dashed line), vertical rolls (dotted lines) and zig-zags (solid line), and experimental values of the excitation thresholds for hexagons, horizontal rolls, vertical rolls and zig-zag pattern (from Ref. [2] with permission). The theoretical curves are evaluated for $l_d = 40\ \mu m,\ \alpha = -0.0134\ cm^2/\mu W$ (see text for definitions).

Though in our system transport is introduced by purpose, we argue that this conclusion has some validity also for physical system in which transport is an intrinsic phenomenon. In hydrodynamical systems subject to Rayleigh-Benard convection, for example, it is well known that a series of transition between different patterns (rolls, cross rolls, zig-zags) occur when increasing the pump parameter [16].

The fact that these hydrodynamical instabilities occur for an increasing pump parameter, represents a relevant difference with our experiment, in which the pattern transitions are observed at fixed pump intensity, varying the transport length Δx. We suggest however that some link between the two situations may exist. On one side, as explicitely discussed in the previous secitions, the instability threshold for pattern formation depends on Δx, and hence modification of Δx at fixed pump intensity results in a modification of the above threshold. On the other side, some hydrodynamical transport lengths can depend on the level of excitation of the system [17]. Following these considerations, we believe that the system here studied belongs to a broader class of physical systems in which nonlocal interactions have a relevant role.

REFERENCES

1. See e.g. F.T. Arecchi. Optical morphogenesis: pattern formation and competition in nonlinear optics, *Il Nuovo Cimento* **107A**, 1111 (1994); *Chaos, Solitons and Fractals*, **4**, 8/9, (Special Issue on *Nonlinear Optical Structures, Patterns, Chaos*), ed. by L.A. Lugiato (1994); *Physica* **D96**, 1/4 (1996).
2. P.L. Ramazza, S. Boccaletti, A. Giaquinta, E. Pampaloni, S. Soria and F.T. Arecchi. Optical pattern selection by a lateral wavefront shift, *Physical Review* **A54**, 3472 (1996).
3. P.L. Ramazza, S. Boccaletti, and F.T. Arecchi. Transport induced patterns in an optical system with focusing nonlinearity, *Optics Communications* **136**, 267 (1997).
4. S.A. Akhmanov, M.A. Vorontsov and V. Yu. Ivanov. Large scale tranverse nonlinear interactions in laser beams; new types of nonlinear waves; onset of "optical turbulence", *JETP Letters* **47**, 707 (1988).
5. G. D'Alessandro and W.J. Firth. Spontaneous hexagon formation in a nonlinear optical medium with feedback mirror, *Physical Review Letters* **66**, 2597 (1991).
6. G. D'Alessandro and W. J. Firth. Hexagonal spatial patterns for a Kerr slice with a feedback mirror, *Physical Review* **A46**, 537 (1992).
7. R. Macdonald and H. J. Eichler. Spontaneous optical pattern formation in a nematic liquid crystal with feedback mirror, *Optics Communications* **89**, 289 (1992).

8. E. Pampaloni, S. Residori and F.T. Arecchi. Roll-hexagon transition in a Kerr-like experiment, *Europhysics Letters* **24**, 647 (1993).
9. E. Pampaloni, P.L. Ramazza, S. Residori and F.T. Arecchi. Two-dimensional crystals and quasicrystals in nonlinear optics, *Physical Review Letters* **74**, 258 (1995).
10. S. Residori, P.L. Ramazza, E. Pampaloni, S. Boccaletti and F.T. Arecchi. Domain coexistence in two-dimensional optical patterns. *Physical Review Letters* **76**, 1063 (1996).
11. E. Pampaloni, S. Residori, S. Soria and F.T. Arecchi. Phase locking in nonlinear optical patterns, *Physical Review Letters* **78**, 1042 (1997).
12. A. Petrossian, L. Dambly and G. Grynberg. Drift instability for a laser beam transmitted through a rubidium cell with feedback mirror, *Europhysics Letters* **29**, 209 (1995).
13. R. Macdonald and H. Danlewski. Self induced optical gratings in nematic liquid crystals with a feedback mirror, *Optics Letters* **20**, 441 (1995).
14. R. Neubecker, G.L. Oppo and T. Tschudi. Pattern formation in a liquid crystal light valve with feedback including polarization, saturation and internal threshold effects, *Physical Review* **A52**, 791 (1995).
15. P.L. Ramazza, P. Bigazzi, E. Pampaloni, S. Residori and F.T. Arecchi. One-dimensional transport induced instabilities in an optical system with nonlocal feedback, *Physical Review* **A52**, 5524 (1995).
16. F.H. Busse and J.A. Whitehead. Instabilities of convective rolls in a high Prandtl number fluid, *Journal of Fluid Mechanics* **47**, 305 (1971).
17. See e.g. P. Manneville, *Dissipative Structures and Weak Turbulence* (Academic Press, London, 1990).